

Fast Feature Matching of UAV Images via Matrix Band Reduction-based GPU Data Schedule

San Jiang^{a,b,c}, Kan You^c, Wanshou Jiang^d, Qingquan Li^{a,b,*}

^a*Guangdong Key Laboratory of Urban Informatics, Shenzhen University, Guangdong Shenzhen, 518060, China*

^b*MNR Key Laboratory for Geo-Environmental Monitoring of Great Bay Area, Shenzhen University, Shenzhen, 518060, China*

^c*Engineering Research Center of Natural Resource Information Management and Digital Twin Engineering Software, Ministry of Education, Wuhan, 430074, China*

^d*State Key Laboratory of Information Engineering in Surveying, Mapping and Remote Sensing, Wuhan University, Wuhan, 430072, China*

Abstract

Feature matching dominates the time costs in structure from motion (SfM). The primary contribution of this study is a GPU data schedule algorithm for efficient feature matching of Unmanned aerial vehicle (UAV) images. The core idea is to divide the whole dataset into blocks based on the matrix band reduction (MBR) and achieve efficient feature matching via GPU-accelerated cascade hashing. First, match pairs are selected by using an image retrieval technique, which converts images into global descriptors and searches high-dimension nearest neighbors with graph indexing. Second, compact image blocks are iteratively generated from a MBR-based data schedule strategy, which exploits image connections to avoid redundant data IO (input/output) burden and increases the usage of GPU computing power. Third, guided by the generated image blocks, feature matching is executed sequentially within the framework of GPU-accelerated cascade hashing, and initial candidate matches are refined by combining a local geometric constraint and RANSAC-based global verification. For further performance improvement, these two steps are designed to execute parallelly in GPU and CPU. Finally, the performance of the proposed solution is evaluated by using large-scale UAV datasets. The results demonstrate that it increases the efficiency of feature matching with speedup ratios ranging from 77.0 to 100.0 compared

*Corresponding Author: liqq@szu.edu.cn

with KD-Tree based matching methods, and achieves comparable accuracy in relative and absolute bundle adjustment (BA). The proposed algorithm is an efficient solution for feature matching of UAV images.

Keywords: unmanned aerial vehicle, oblique photogrammetry, cascade hashing, feature matching, Structure from Motion, bundle adjustment

1. Introduction

Unmanned aerial vehicle (UAV) has been increasingly becoming a critical remote sensing platform in photogrammetry and computer vision (Jiang et al., 2021b; Yao et al., 2019), and it has been widely used in a range of applications, e.g., indoor inspection of transmission lines (Jiang et al., 2017), procedural 3D modeling of urban facilities (Wang et al., 2023), and precision management of agricultural plants (Zheng et al., 2021). The precise calculation of camera poses is an essential preliminary step, which has been usually implemented through structure from motion (SfM) (Jiang et al., 2020a). In the workflow of SfM, the time costs are dominated by feature matching due to the quadratic combination complexity of match pairs and nearest neighbor searching (NNS) of high-dimension feature descriptors. Thus, fast feature matching is required for recent SfM systems.

In the literature, extensive work has been reported to address these issues. To decrease the combination complexity of match pairs, auxiliary data and visual similarity are the widely used clues to select overlapped image pairs and avoid exhaustive feature matching (Hartmann et al., 2016), e.g., the on-board POS (Positioning and Orientation System) data from UAV platforms (Jiang and Jiang, 2020; Remondino and Gerke, 2015) and the geometric priors from data acquisitions (Jiang et al., 2024; Schönberger et al., 2014). In addition, to cope with oblique data acquisition and geometry-aware trajectory planning (Li et al., 2023), visual similarity has also been extensively exploited in modern SfM systems, which usually use pre-trained visual words to encode images into fix-length vectors and convert the problem of selecting overlapped image pairs into the one of nearest neighbor searching among the vectors, such as BoW (Bag-of-Words) (Nister and Stewenius, 2006; Havlena and Schindler, 2014; Jiang et al., 2022a) and VLAD (Vector of Locally Aggregated Descriptors) (Hou et al., 2023; Jiang et al., 2023). By using these techniques, the time complexity of feature matching is significantly decreased, which is transited from a quadratic relationship to a linear one with respect

to the number of involved UAV images.

Match pair selection reduces the combination complexity of images. However, high time costs are still required in the exhaustive nearest neighbor searching among two sets of high-dimension feature descriptors (Hartmann et al., 2016), especially for the widely used KD-Tree based SIFT feature matching (Lowe, 2004). To accelerate feature matching, existing methods can be divided into two groups, i.e., redesign of feature descriptors and acceleration of feature matching. For the former, feature descriptors are designed to decrease the computational burden, such as the ORB (Rublee et al., 2011) with binary descriptors. However, as verified in recent work, SIFT-based feature matching is still the most robust algorithm in practical engineering applications (Ji et al., 2023; Jiang et al., 2021a). For the latter, the hardware acceleration technique has been exploited to speed up feature matching. The classical examples include the SIFTGPU (Wu, 2011) and popsift (Griwodz et al., 2018) algorithms that exploit GPU (Graphic Processing Unit) for feature matching. In contrast to the KD-Tree based approximate nearest neighbor (ANN) searching, hashing-based methods have also gained lots of attention in feature matching, whose core idea is to convert the real-value descriptors to discrete binary codes via hashing functions and map similar descriptors of query and database images into the same cell (Cheng et al., 2014). To achieve higher speedup ratios, GPU acceleration and data schedule have been integrated into hashing-based matching pipelines in the recent work (Xu et al., 2017; Zhang et al., 2023), which use hardware acceleration for calculating hash codes and similarity scores and exploit data schedule to relief input/output (IO) burdens.

Compared with classical SIFT matching algorithms, hashing-based methods can achieve promising speedup ratios for feature matching of UAV images. However, some issues still exist in the proposed solutions. First, the performance of existing data schedule depends on the connection structures between images. In the work of Xu et al. (2017), the group-block based data schedule strategy assumes dense image connections. For oblique photogrammetry, image connections are usually very sparse, and it degenerates the overall performance of GPU-based hashing matching. Second, existing data schedule strategies emphasize more on the IO burdens, however, ignoring the parallel computing power of modern GPU. For the data schedule used in Zhang et al. (2023), image loading and free sequences are first generated based on the image connection structure, and feature matching is executed sequentially according to loading and free sequence. In other words, only one

image is matched against other images in GPU memory. Third, outliers are prone to retain in feature matching due to the usage of binary hashing codes for calculating descriptor similarity scores. It would cause high time cost in classical RANSAC (Random Sample Consensus) based outlier removal (Lu et al., 2016). Thus, this study proposes a matrix band reduction-based GPU data schedule for fast feature matching of UAV images. Our main contributions are summarized as follows: (1) we propose a matrix band reduction (MBR) based data schedule strategy to divide the sparsely connected view graph into compact blocks, which can adapt well to the connection structure of images and the memory volume of GPUs; (2) we design a cascade hashing based feature matching workflow that integrates the spatial angular order (SAO) based local constraint and RANSAC-based global verification for outlier removal. Combined with MBR-based data schedule, the proposed image matching solution can increase the usage of GPU for feature matching and CPU for outlier removal; (3) we verify the performance of the proposed feature matching solution by using large-scale datasets and compare it with state-of-the-art software packages.

This paper is organized as follows. Section 2 presents the workflow of the GPU data schedule algorithm for efficient feature matching of UAV images. 3 conducts the performance evaluation and comparison with other methods. Finally, Section 4 presents the conclusions.

2. Methodology

This study proposes a fast feature matching of UAV images via matrix band reduction-based GPU data schedule as shown in Figure 1. There are three major steps, i.e., view graph construction, schedule block generation, and cascade hashing feature matching. First, SIFT features are extracted from each image and used to calculate VLAD-based image descriptors using a pre-trained codebook. After indexed in the HNSW (Hierarchical Navigable Small World) based graph structure, overlapped image pairs are retrieved and used to construct the view graph. Second, the initial view graph is first compressed through a matrix band reduction algorithm, which permutes the image order and ensures that overlapped match pairs are located near the diagonal region in the view graph. Data schedule blocks are then created from the permuted adjacent matrix. Through the iterative execution of MBR, a list of schedule blocks can be generated. Finally, images in each schedule block are loaded into GPU memory for calculating hashing codes and

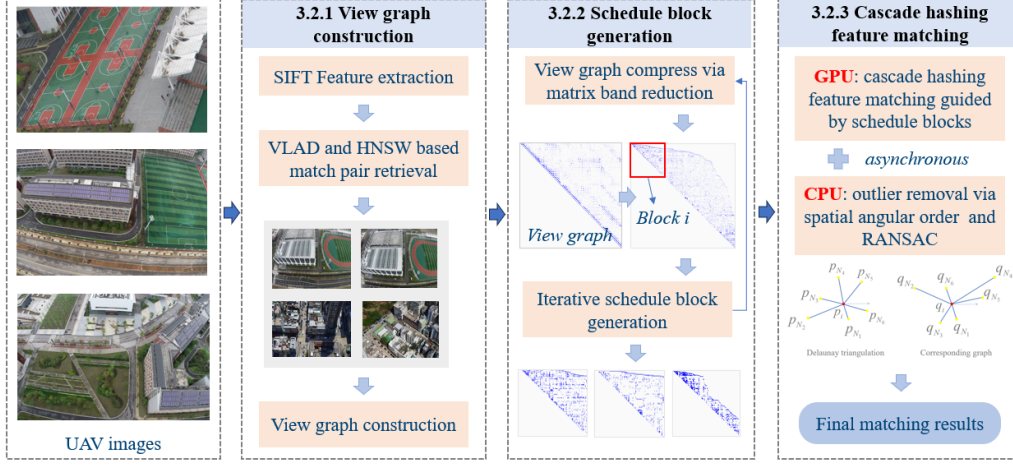


Figure 1: The workflow of the proposed algorithm.

generating initial matching results. At the same time, outlier removal is simultaneously conducted on the CPU by using spatial angular order-based local geometric constraint and RANSAC-based global geometric constraint. The details are presented in the following sections.

2.1. Overview of cascade hashing feature matching

Hashing-based feature matching converts real-value feature descriptors to binary hashing codes, and the similarity scores of feature descriptors can be calculated through a bit-wise XOR operation at a fast speed. In contrast to a single-layer structure, cascade hashing adopts a three-layer structure to implement coarse-to-fine feature matching (Cheng et al., 2014), as shown in Figure 2. Because of the data-independent characteristic, LSH (Locality Sensitive Hashing) has been used as the hashing function in cascade hashing feature matching. Cascade hashing feature matching includes four steps:

(1) Hashing lookup with multiple tables. All feature descriptors in each image are mapped into m bits short binary codes using LSH with L sets of random hashing functions. For each set of hashing functions in L , a lookup table is created by using 2^m buckets. Thus, for query point p in image I , all points that fall into the same bucket of p in image J are returned as its candidate matches.

(2) Hashing remapping for fine encoding. m bits coarse hashing increases the recall of feature matching while the precision is low. Thus,

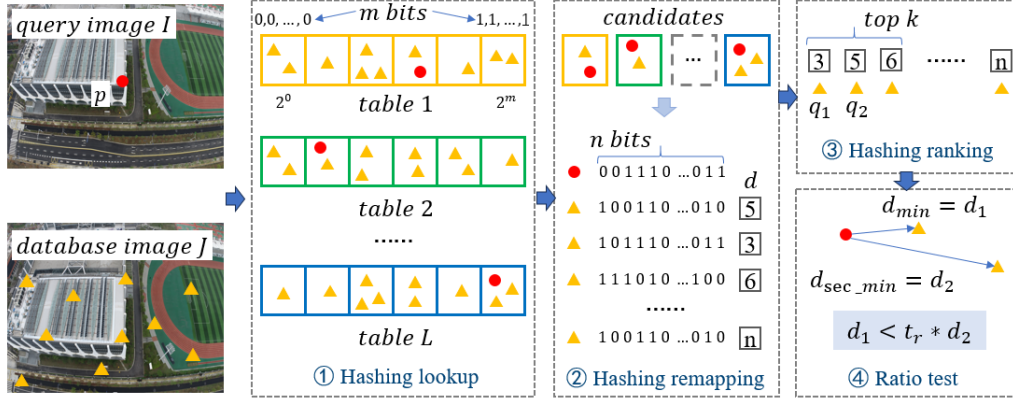


Figure 2: The principle of cascade hashing feature matching.

candidate matches are remapped into n ($n > m$) bits long binary codes with LSH. The Hamming distance that ranges from 0 to n is computed between the query point p and their candidate matches, and it is used to sort candidate matches ascndly.

(3) Hashing ranking for top-K nearest neighbors. To achieve efficient NNS, hashing buckets with the Hamming distance as keys are established for all candidate matches. Nearest neighbors are returned by sequentially checking buckets until the number of returned matches reaches K .

(4) Euclidean distance calculation and ratio test. Hamming distances of hashing codes have lower precision than Euclidean distances of feature descriptors. For the top-K candidate matches, their Euclidean distances to the query point are calculated. The nearest neighbor q_1 and second nearest neighbor q_2 are determined, and q_1 that passes the ratio test $dis(q_1) < dis(q_2) * t_r$ is labeled as a final match. t_r is the ratio test threshold, and $dis(*)$ indicates the distance to the query point.

According to cascade hashing feature matching, feature matches between images I and J can be established. As in Cheng et al. (2014), the default parameters are used in this study. That is, the number of tables $L = 6$; the number of bits for coarse and fine encoding is set as $m = 8$ and $n = 128$, respectively; and the number of nearest neighbors is set as $K = 8$. Noticeably, in ANN-based feature matching, the ratio test threshold t_r balances the precision and recall of final matches, which is set as 0.8 in SIFTGPU. However, for cascade hashing matching, candidate matches have been selected in the coarse matching step (3). Thus, a proper t_r would be evaluated.

2.2. Matrix band reduction-based GPU data schedule for feature matching

GPU-accelerated cascade hashing gains extremely high efficiency. However, the hard disk to GPU data schedule and limited volume of GPU memory degenerates its overall performance. Although promising efficiency has been reported in recent studies (Xu et al., 2017; Zhang et al., 2023), these methods either rely on dense image connections or not fully exploit the computing power of modern GPU. Therefore, this study proposes a matrix band reduction-based GPU data schedule for fast feature matching, which aims to adapt to both densely and sparsely connected images and use GPU computing power as high as possible.

2.2.1. View graph construction based on image retrieval

Match pairs are first selected to create a view graph that would be used for data schedule between hard disk and GPU memory and guide feature matching. Although on-board POS data can be used as useful clues for efficient match pair selection, this method depends on the precision of onboard sensors and cannot adapt to geometry-aware data acquisition, e.g., optimized views photogrammetry. Instead, visual similarity-based image retrieval has gained more attention, and BoW-based image retrieval encodes feature descriptors as vectors by using a pre-trained codebook and casts match pair selection as the problem of searching the nearest neighbors among BoW vectors. It has been implemented in commercial and open-source software packages. However, its efficiency decreases dramatically for large-scale UAV images due to the large number of extracted features and the large-size codebook required for encoding large-scale datasets.

To address this challenge, the study employs a high-efficiency image retrieval framework (Jiang et al., 2023). The proposed methodology integrates two core components: (1) the VLAD representation for compact image encoding, and (2) the HNSW graph structure for efficient vector indexing. The VLAD descriptor utilizes a minimal-size codebook to aggregate local feature descriptors into a unified high-dimensional global representation, significantly reducing computational redundancy. Concurrently, the HNSW index architecture accelerates the approximate nearest neighbor search process over the encoded VLAD vectors, enabling rapid similarity matching while maintaining sublinear time complexity. This synergistic combination balances representational compactness with scalable search performance.

According to the VLAD-HNSW based image retrieval, a set of match pairs $P = \{p_{ij}\}$ are selected and used to create the view graph. Suppose that there

are n images, the view graph is constructed as an adjacent matrix M_{ij} , $i = 1, 2, \dots, n; j = 1, 2, \dots, n$. For each match pair p_{ij} , set corresponding item $M_{ij} = 1$; otherwise, set $M_{ij} = 0$. In this study, the view graph M_{ij} would be used to generate blocks for data schedule and guide feature matching.

2.2.2. Schedule block generation via iterative matrix band reduction

Data schedule between hard disk and GPU is required since all feature descriptors cannot be loaded into GPU with limited memory at one time. In general, existing strategies for data schedule can be grouped into three categories. The most direct strategy is to execute feature matching sequentially for all selected match pairs. This strategy, however, causes frequent data load and free in GPU. For the second category, data load and free lists are first generated according to their connections, and feature matching is conducted by the interleaved execution of reading in data in the load list and clearing out data in the free list. This strategy decreases data schedule burdens. However, it does not fully exploit the computing power of GPU since only the newly loaded image is matched with other images in GPU. For the third category, images are divided into blocks that can be loaded into GPU at one time, and feature matching is then executed between loaded images. It has high efficiency in pair-wise feature matching. For sparsely connected images, its performance decreases obviously.

Inspired by recent work, this study proposes a data schedule strategy based on iterative matrix band reduction. The core idea is to reduce the bandwidth of the original adjacent matrix M_{ij} via a matrix band reduction algorithm and generate schedule blocks from the compressed MBR matrix under the limitation of GPU memory. In the matrix theory, matrix band reduction, often referred to as bandwidth reduction, is a technique used in numerical analysis to optimize the storage and computational efficiency of sparse matrices. The band of a matrix consists of the diagonal and the rows and columns immediately adjacent to it, which contain the non-zero elements of the matrix. Figure 3 illustrates the effect of MBR. The original adjacent matrix M_{ij} has sparse image connections that are rendered by blue color and distributed over the whole matrix space, as shown in Figure 3(a). After applying MBR, the image connections are recorded and located near the diagonal as near as possible, as shown in Figure 3(b). In other words, MBR consolidates the non-zero elements of a sparse matrix into a tighter central region around the diagonal and makes them easier to manage.

Based on the basic idea of MBR, this study implements a data schedule

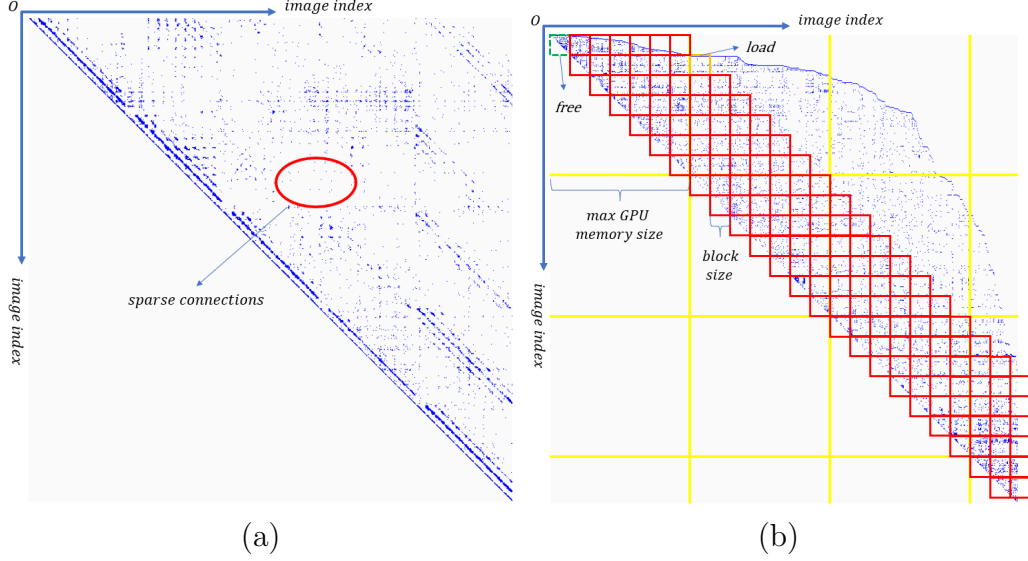


Figure 3: The illustration of schedule block generation based on matrix band reduction: (a) original adjacent matrix; (b) compressed MBR matrix. The blue color indicates connected image pairs while the white color means no connection between corresponding images.

strategy according to the following steps:

(1) Initialization. A symmetrical adjacent matrix M_{sym} is constructed from the original adjacent matrix M_{ij} , and an image id list $list_{id}$ is generated by using image indices that are deduced from rows or columns of M_{ij} .

(2) Calculate permute order. By using the MBR algorithm, a permute order $order_{perm}$ is generated, which permutes the row and column index of M_{sym} and creates the MBR matrix M_{mbr} . This study adopts the Gibbs-Poole-Stockmeyer (GPS) algorithm (Gibbs et al., 1976) due to its low time costs and memory requirements. In addition, the image id list $list_{id}$ is updated according to $order_{perm}$.

(3) Create new schedule blocks. By using MBR matrix M_{mbr} , new schedule blocks are created under the limitation of the GPU memory. As presented in Figure 3(b), the GPU memory size $Size_{gpu}$ is restricted by the yellow grids, which indicates the maximum number of descriptor data that can be loaded into GPU memory. By defining the block size $Size_{blk}$, new schedule blocks $block_{ij}$ are created as rendered by red rectangles in Figure 3(b), in which i and j represents the row and column index of each block, respectively. Block $\{block_{ij}\}$ stores its corresponding match pairs.

(4) **Update adjacent matrix and image id list.** After feature matching guided by schedule blocks $block_{ij}$, the MBR matrix M_{mbr} is updated by setting the cell value of the corresponding match pairs as zero and removing the rows and columns that have no match pairs. Besides, image id list $list_{id}$ is updated accordingly.

(5) **Termination.** Iteratively executing steps (2)-(4) until the MBR matrix M_{mbr} is empty. Finally, the schedule blocks $\{block_{ij}\}$ can be obtained.

Compared with existing data schedule strategies, the proposed solution has two major advantages. First, it can minimize data load and free in GPU as much as possible because of the usage of MBR algorithm for adjacent matrix compression and block generation; second, a high usage ratio of GPU can be achieved because match pairs as many as possible are packed into one schedule block.

2.2.3. Cascade hashing matching enhanced by geometric constraints

Cascade hashing feature matching is then implemented using the generated data schedule blocks $\{block_{ij}\}$. As the sum of data volume in each block row i is restricted by GPU memory, feature descriptors in the block row can be loaded into GPU at one time. Supposing that generated blocks $\{block_{ij}\}$ consists of k rows and l columns, i.e., $i = 1, 2, \dots, k$ and $j = 1, 2, \dots, l$, and the current block row is represented as $\{block_{i1}, block_{i2}, \dots, block_{il}\}$. The pipeline of cascade feature matching is implemented as follows:

(1) **Load feature descriptors from block.** Feature descriptors corresponding to match pairs in each block are sequentially loaded into GPU, and their hashing codes and bucket ids are simultaneously computed to build hashing lookup tables.

(2) **Execute cascade hashing matching.** Based on the established hashing lookup tables, hashing feature matching is executed and guided by match pairs, and initial matches that pass through the ratio test are retained.

(3) **Free unnecessary data block.** Iteratively execute steps (1) and (2) until all blocks in the current block row are processed. The data in the first block $block_{i1}$ is free as it would not be used in the next block row.

For each block row $\{block_{i1}, block_{i2}, \dots, block_{il}\}$, the above pipeline is executed to obtain initial candidate matches for all related match pairs. Noticeably, in step (1), redundant data loading operations can be avoided. As illustrated in Figure 3(b) for processing the second block row, only descriptors in the last block $block_{il}$ rendered in orange color should be loaded into GPU since all the other required data has been loaded when processing the

first block row. Besides, after processing each block row, data in the first block $block_{i1}$ rendered in green color is free as in step (3). The interleave free-load operation goes through the whole pipeline.

False matches inevitably existed in initial matches due to limited discriminability of local feature descriptors and large perspective deformations. In this study, outlier removal is finally conducted by combining the spatial angular order (SAO) based local geometric constraint and RANSAC-based global geometric constraint (Jiang et al., 2020b). The local geometric constraint is designed by using the k-nearest neighbors deduced from the Delaunay triangulation and its corresponding graph. To achieve further efficiency improvement, outlier removal is simultaneously executed in CPU after obtaining initial matches in step (2). Thus, the results retained in outlier removal are the final matches.

2.3. Algorithm implementation

According to the workflow shown in Figure 1, this study implements the proposed cascade hashing matching algorithm by using the C++ programming language. For match pair retrieval, SIFTGPU (Wu, 2011) with default parameters is utilized to extract SFIT features, and Lloyd’s K-means cluster algorithm (Lloyd, 1982) is adopted to cluster selected training descriptors for the codebook construction. Besides, with the aid of VLFeat (Vedaldi and Fulkerson, 2010) and FAISS packages (Johnson et al., 2019), we have implemented the VLAD-HNSW based image retrieval solution. To facilitate performance evaluation in SfM reconstruction, the cascade hashing feature matching solution has been integrated into the SfM engine in Jiang et al. (2022b). The pseudo-code is presented in Algorithm 1.

3. Experimental results

3.1. Datasets and software packages

Three UAV datasets are collected in study for performance evaluation. The details of data acquisitions and collected images are presented in Table 1 and described as follows.

- The first dataset comprises 3,743 images over a university campus, as presented in Figure 4(a). These images are obtained by using a DJI Phantom 4 RTK UAV, which is equipped with a DJI FC6310R camera. Each image has 5,472 by 3,648 pixels and is taken at a flight altitude of 80 m, yielding a Ground Sample Distance (GSD) of about 2.6 cm.

Algorithm 1 cascade hashing feature matching

Input: UAV images $I = \{i_i\}$ of size n

Output: Feature matching results $match = \{m_{ij}\}$

```
1: procedure VIEWGRAPHCONSTRUCTION
2:   Extract SIFT features for each image  $i_i \in I$ 
3:   Select a subset of  $p$  percent of images from  $I$  as training images  $I_p$ 
4:   Add top-scale  $h$  features of image  $i_i \in I_p$  to training descriptors  $D_t$ 
5:   Generate a codebook  $C$  with  $k$  words using training descriptors  $D_t$ 
6:   Retrieve match pairs  $P = \{p_{ij}\}$  via VLAD-HNSW
7:   Create View graph  $M_{ij}$  using selected match pairs  $P$ 

1: procedure CASCADEHASHINGMATCHING
2:   Initialize symmetrical matrix  $M_{sym}$  and image id list  $list_{id}$  from  $M_{ij}$ 
3:   while  $M_{sym}$  is not empty do
4:     Assign schedule blocks  $block = \{\}$ 
5:     Calculate permute order  $order_{perm}$  from symmetrical matrix  $M_{sym}$ 
6:     Create MBR matrix  $M_{mbr}$  and update list  $list_{id}$  using  $order_{perm}$ 
7:     Create schedule blocks from  $M_{mbr}$  and add to  $block \leftarrow \{block_{ij}\}$ 
8:     Update symmetrical matrix  $M_{sym} = M_{mbr}$ 
9:     for each  $\{block_{i1}, block_{i2}, \dots, block_{il}\} \in block$  do
10:      Load descriptors in current block  $block_{ij}$ 
11:      Execute cascade hashing matching for  $block_{ij}$ 
12:      Remove outliers and store results  $match \leftarrow \{m_{ij}\}$ 
13:      Free unnecessary data in block  $block_{i1}$ 
14:      Set matrix  $M_{sym}$  cells as zero for processed pairs
```

- The second dataset encompasses 4,030 images from a complex university building as shown in Figure 4(b). These images are captured by a DJI M300 RTK UAV, equipped with a DJI Zenmuse P1 camera that produces images with dimensions of 8,192 by 5,460 pixels. The dataset has been collected by using optimized views photogrammetry (Li et al., 2023), which adjusts camera orientation according to geometric attributes of terrestrial objects. The GSD is about 1.2 cm. For absolute orientation, 26 Ground Control Points (GCPs) have been gathered using a total station, which offers a nominal precision of 0.8 cm and 1.5 cm in the horizontal and vertical direction, respectively.
- The third dataset is captured from a test site that is predominantly

Table 1: Detailed information about the three UAV datasets.

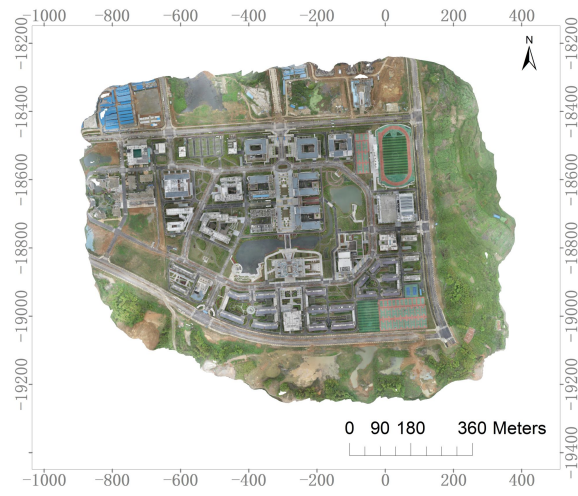
Item Name	Dataset 1	Dataset 2	Dataset 3
UAV type	multi-rotor	multi-rotor	multi-rotor
Flight height (m)	80.0	-	87.0
Camera mode	DJI FC6310R	DJI ZenmuseP1	SONY ILCE 7R
Number of cameras	1	1	5
Focal length (mm)	24	35	35
Camera angle (°)	0	-	Nadir: 0; oblique: 45/-45
Number of images	3,743	4,030	21,654
Image size (pixel)	5472×3648	8192×5460	6000×4000
GSD (cm)	2.6	1.2	1.2

Table 2: The configuration of the evaluated methods. The term VOC-Tree indicates vocabulary tree-based image retrieval.

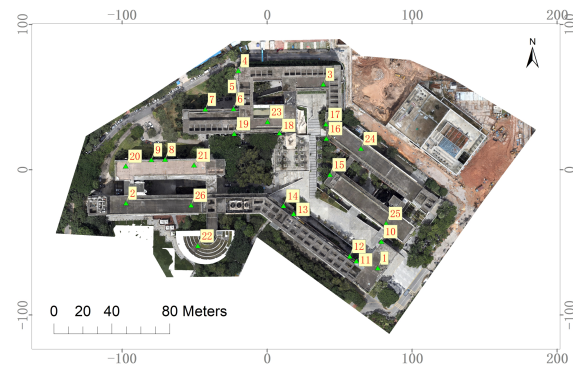
Method	Match pair selection	Feature matching algorithm	Data schedule	Hardware acceleration	Software version
ColMap-CPU	Input pairs	KD-Tree	No	Multi-core CPU	3.10
ColMap-GPU	Input pairs	NNS	Yes	GPU & CPU	3.10
AliceVision	Input pairs	Cascade hashing	No	Multi-core CPU	v2023.3.0
TLBDS	Input pairs	Cascade hashing	Yes	GPU & CPU	/
Metashape	POS	/	Yes	GPU & CPU	1.8.21
Pix4Dmapper	VOC-Tree	/	Yes	GPU & CPU	4.4.12
Ours	Input pairs	Cascade hashing	Yes	GPU & CPU	/

characterized by low-rise structures and an abundance of dense vegetation, with a river flowing through the area as shown in Figure 4(c). For data acquisition, a typical penta-view oblique photogrammetry with five SONY ILCE 7R cameras has been adopted, which record images with dimensions of 6,000 by 4,000 pixels. At an altitude of 87.1 m, a collection of 21,654 images is gathered, achieving a GSD of 1.2 cm.

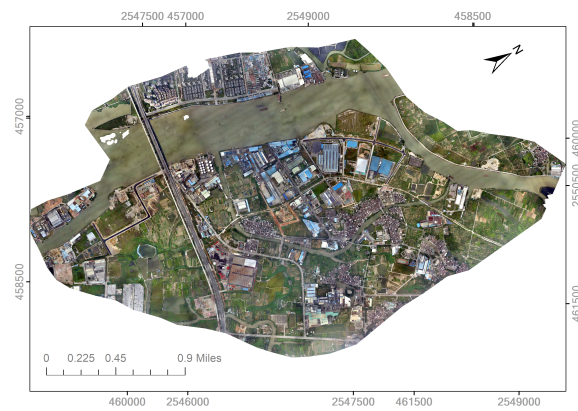
For performance evaluation, this study compares the proposed algorithm with five well-known software packages, as listed in Table 2, including two open-source software packages ColMap (Schonberger and Frahm, 2016) and



(a) Dataset 1



(b) Dataset 2



(c) Datasets 3

Figure 4: The orthomosaics of the three test sites.

AliceVision (Griwodz et al., 2021), two commercial software packages Metashape (Agisoft, 2024) and Pix4Dmapper (Pix4Dmapper, 2024), and one recently cascade hashing matching algorithm, termed TLBDS (Zhang et al., 2023). In the experiments, all tests are conducted on a Windows platform equipped with 64 GB memory, a 3.0 GHz Intel Core i9-13900K CPU and a 24 GB NVIDIA GeForce RTX 4090 graphic card.

3.2. Analysis of schedule block size and ratio test threshold on feature matching

In the proposed cascade hashing based feature matching algorithm, the schedule block size $Size_{blk}$ and ratio test threshold t_r are two critical parameters. The schedule block size determines the quantity of data that is loaded and free while processing each block row and the count of match pairs that are fed to GPU to perform feature matching. For a small block size, the load and free of data are consistently less demanding, which in turn results in reduced GPU usage. Conversely, a large block size can process more matching pairs simultaneously, thereby increasing the GPU usage and data scheduling demands. Meanwhile, the ratio test threshold determines the number of initial matches that are retained in cascade hashing feature matching. In contrast to global NNS, candidate matches have been filtered in the coarse matching step, which leads to the practical threshold used in the other algorithm is not proper. Thus, we will analysis their influence on feature matching and select their optimal values.

For the analysis of schedule block size $Size_{blk}$, datasets 1 and 2 are selected as they are captured by using two different photogrammetric configurations, which results in the collected images with varying viewing directions and image overlap degrees. In this test, the schedule block size is sampled with the values of 50, 100, 150, 200, 400, 600, and 800 under the limitation of the maximum GPU memory, and time cost is used as the metric for performance evaluation. The results are shown in Figure 5. It is clearly shown that the time cost decreases consistently with the increase of schedule block size ranging from 50 to 400. The main reason is that for the large block size, more match pairs are fed to GPU at one time, which would increase the GPU usage and in turn increase matching efficiency. Noticeably, higher efficiency improvement is observed from dataset 2 when compared with that in dataset 1. It can be explained by the larger image overlap degree in dataset 2. When the schedule block size further increases from 400 to 800, it is shown that the time cost almost keeps constant for these two datasets because of the

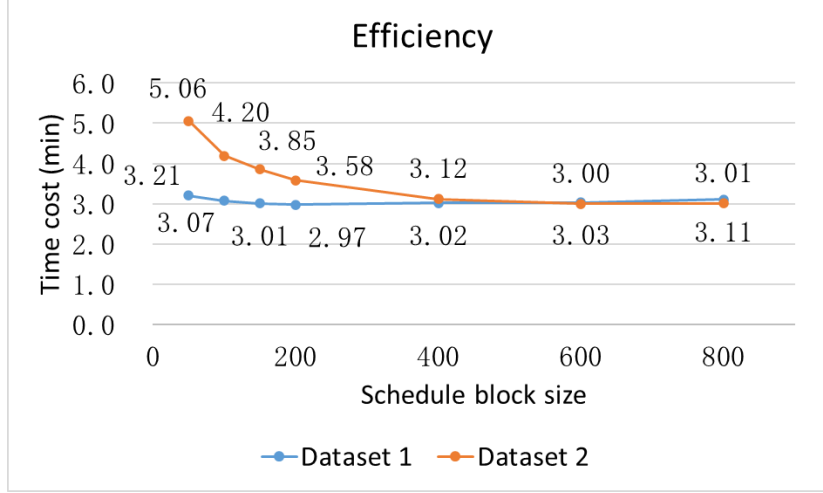
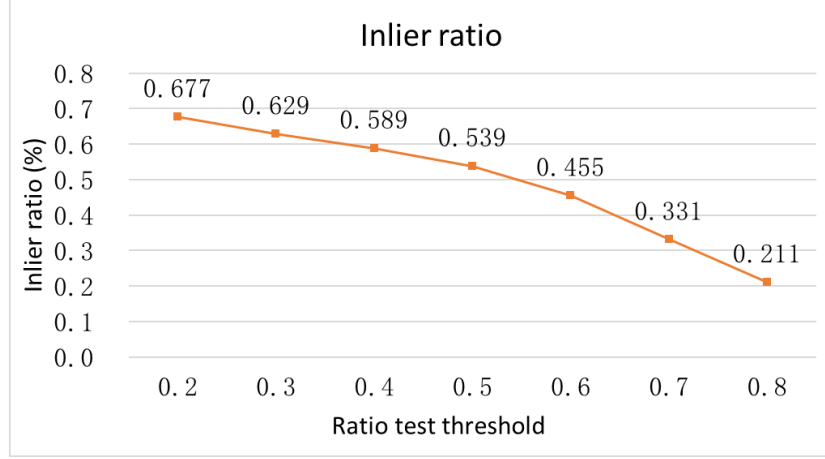


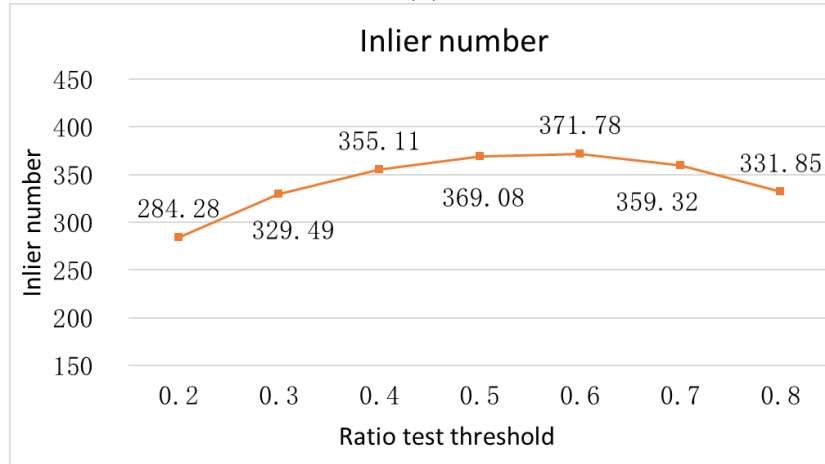
Figure 5: The influence of the schedule block size on matching efficiency.

full usage of the maximum GPU computing power. Therefore, $Size_{blk}$ is configured as 400 in the following tests.

For the analysis of ratio test threshold t_r , dataset 2 is selected for tests due to the existence of different and classical structures. In this test, the ratio test threshold is sampled from 0.2 to 0.8 with an interval value of 0.1. The inlier ratio and inlier number are used as the metrics for performance evaluation. The former is the ratio between the number of inliers and all matches; the latter is the number of true matches after outlier removal. Figure 6 presents the results. We can see that with the increase of ratio test threshold, the inlier ratio continuously decreases from 0.677 to 0.211, as shown in Figure 6(a). The main reason is that more outliers pass the ratio test with the increase of the ratio test threshold when compared with the number of inliers. For the results in Figure 6(b), the change of the inlier number can be divided into two stages. In the first stage, it increases from 284.28 to 371.78 for the threshold increasing from 0.2 to 0.6. The main reason is that more matches pass the ratio test, which in turn increases the inlier number. On the second stage ranging from 0.6 to 0.8, the inlier number continuously decreases as the lower inlier ratio degenerates the performance of subsequent outlier removal. For a visual analysis, Figure 7 presents the feature matching result of one image pair under varying threshold. Thus, for a balance between inlier ratio and inlier number, t_r is set as 0.5 in the following test.



(a)



(b)

Figure 6: The influence of the ratio test threshold on inlier ratio and inlier number using dataset 2: (a) average inlier ratio; and (b) average inlier number.

3.3. Analysis of the key steps of the proposed feature matching workflow

Match pair selection is the first step of the proposed feature matching workflow. In this study, the HNSW-VLAD based image retrieval technique has been used to achieve efficient match pair selection for the three datasets. Three metrics, i.e., *efficiency*, *precision*, and the *number of match pairs*, are used for performance evaluation. The first one indicates the time cost in image retrieval; the second one is the ratio between the number of true match

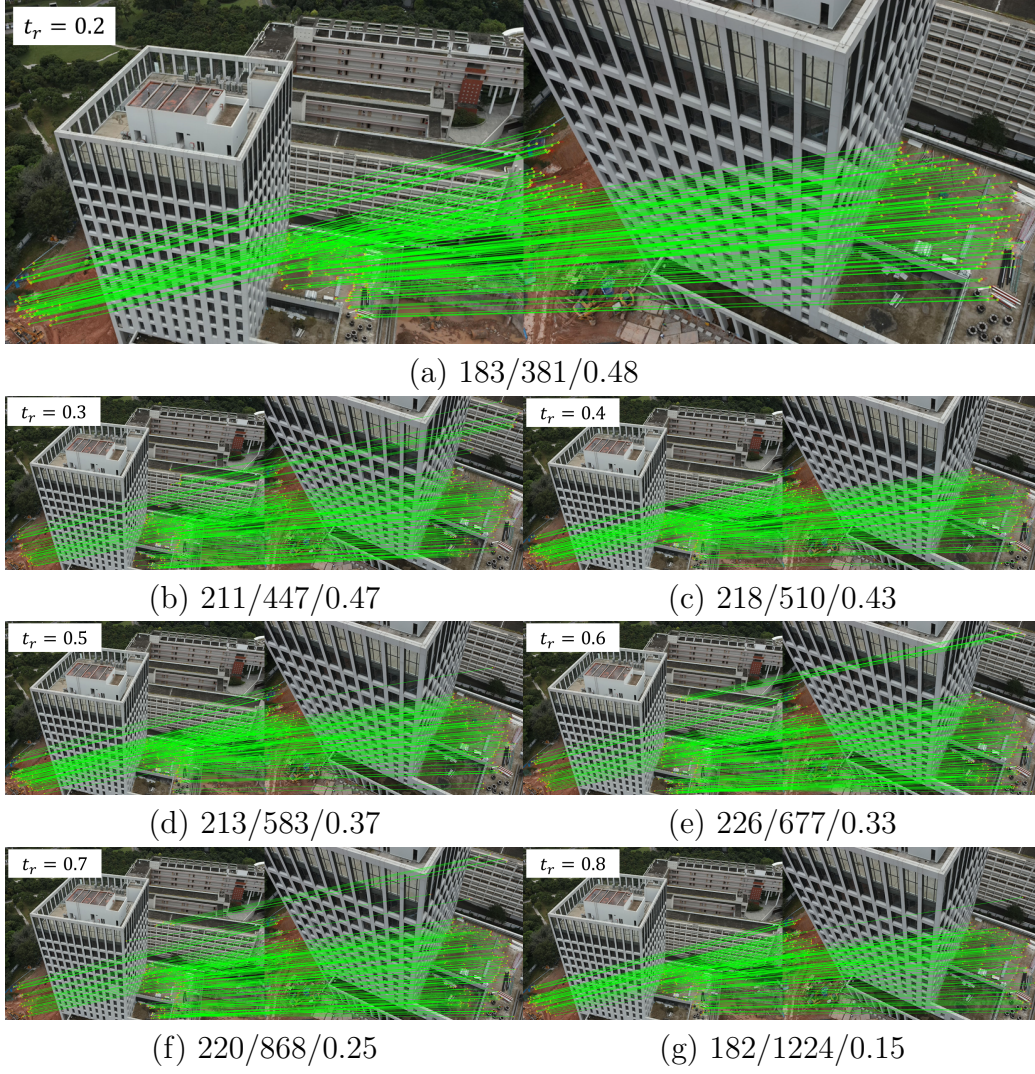


Figure 7: Feature matching results of one image pair in dataset 2 under different ratio test threshold t_r . The values along with the title of each sub-figure indicate the number of inliers and initial matches and its corresponding inlier ratio. Noticeably, presented results are final matches after outlier removal.

Table 3: The statistical results of match pair selection for the three datasets in terms of efficiency, precision, and the number of match pairs.

Metric	Dataset 1	Dataset 2	Dataset 3
Efficiency (min)	1.0	1.2	8.8
Precision (%)	89.8	89.0	96.0
Number of match pairs	61,762	67,787	366,799

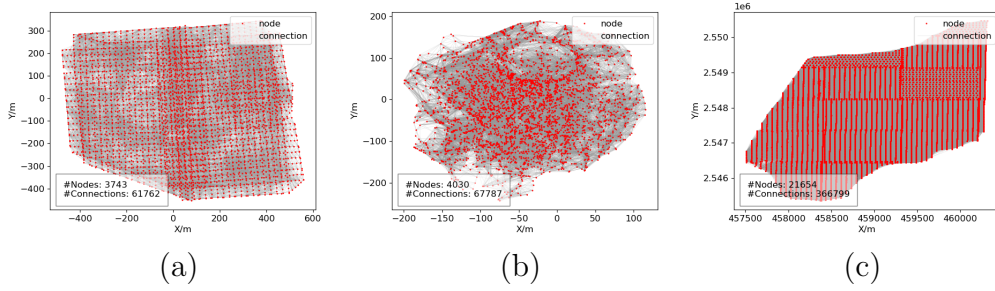


Figure 8: Image connection network created from match pairs: (a) dataset 1; (b) dataset 2; (c) dataset 3. Red dots and gray lines respectively indicate images and connections.

pairs and all retrieved match pairs. The statistical results are presented in Table 3. We can conclude that for the three datasets there are a total number of 61,762, 67,787, and 366,799 match pairs selected under the time costs of 1.0 min, 1.2 min, and 8.8 min, respectively. In other words, the average time cost is almost independent of the data volume, which is approximately 0.97 ms, 1.06 ms, and 1.44 ms for the three datasets, respectively. In addition, the metric *precision* for the three datasets is 89.8%, 89.0%, and 96.0%, which ensures high precision for the retrieved match pairs to create the subsequent view graph, as shown in Figure 8. Thus, the proposed algorithm can easily scale to very large-scale UAV datasets.

View graphs can then be constructed using the retrieved match pairs and used to achieve the schedule block generation and guide cascade hashing feature matching. In the proposed schedule block generation algorithm, the view graph is indicated as the adjacent matrix created from match pairs and MBR matrix by executing matrix band reduction. The former creates the initial connection relationship of original images; the latter represents the compressed structure of permuted images, which is used to facilitate schedule block generation. Figure 9 shows the adjacent matrix and MBR

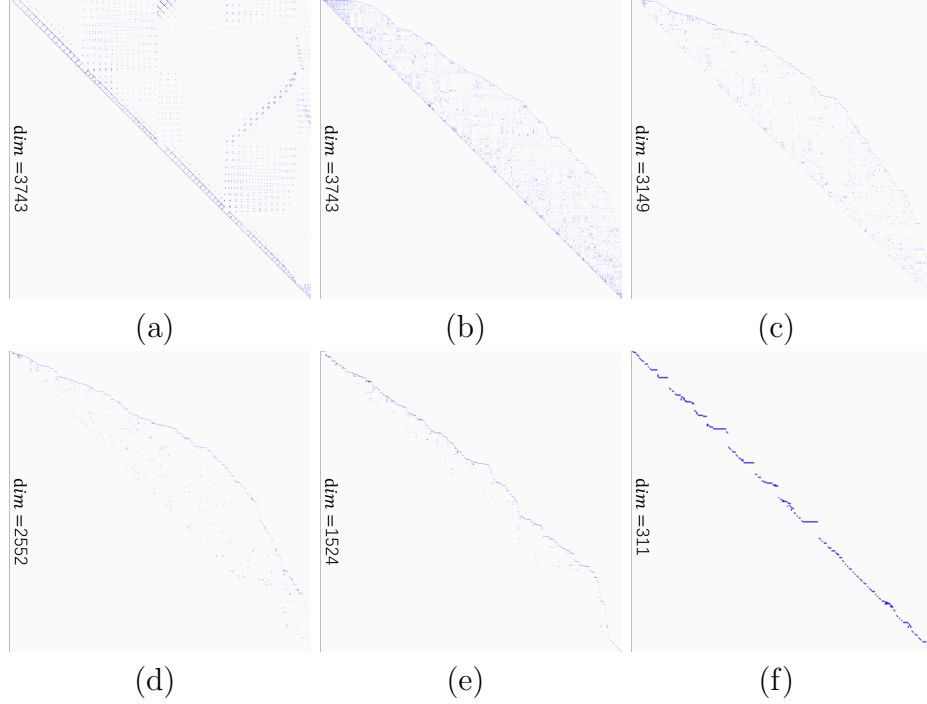


Figure 9: The adjacent matrix and MBR matrix in schedule block generation for dataset 1: (a) adjacent matrix at initialization; (b) MBR matrix at iteration 1; (c) MBR matrix at iteration 2; (d) MBR matrix at iteration 3; (e) MBR matrix at iteration 4; (f) MBR matrix at iteration 5. The term *dim* at the left border of each sub-figure indicates the row and column size of the matrix.

matrix during cascade hashing feature matching, in which blue dots indicate corresponding connected images. As shown in Figure 9(a), retrieved match pairs have very sparse connections, as represented by spare blue dots. After applying matrix band reduction at iterations 1, 2, 3, 4, and 5, the MBR matrix shows very compact connections that are almost near the matrix diagonal, as shown in Figure 9(b) to Figure 9(f). Noticeably, during the proceeding of executing feature matching, the dimension of the MBR matrix also decreases from 3743 at iteration 1 to 311 at iteration 5. The main reason is that after feature matching, the images without any other overlapped images have been removed from the MBR matrix. Finally, the dimension of the MBR matrix becomes zero since all match pairs are processed. Therefore, it verifies the correction of the proposed data schedule strategy.

To verify the effectiveness of the proposed data schedule strategy, this

Table 4: The comparison of feature matching efficiency without and with data schedule. The unit of speed is pairs/s.

Dataset	No schedule		Schedule		Speedup
	Time (s)	Speed	Time (s)	Speed	
1	3260.22	18.94	181.20	340.85	17.99
2	2946.06	23.01	187.20	362.11	15.74
3	15766.86	23.26	1602.06	228.95	9.84

study compares feature matching efficiency without and with the data schedule. The only difference between these two tests is the usage of the data schedule strategy. The performance is evaluated by the metrics *time* and *speed*, which are quantified respectively by time costs of feature matching and the number of pairs processed per second. Table 4 presents the results. It is shown that when not using the data schedule strategy, the matching speed is merely 18.94 pairs/s, 23.01 pairs/s, and 23.26 pairs/s, respectively; on the contrary, by using the data schedule strategy, the matching speed improves obviously, which reaches to 340.85 pairs/s, 362.11 pairs/s, and 228.95 pairs/s for each dataset. In other words, the speedup ratio is 17.99, 15.74, and 9.84 for the three datasets, respectively. It can be explained by frequent IO burdens in data load and the low GPU usage for sequential feature matching. Thus, the proposed data schedule strategy improves the efficiency of cascade hashing feature matching.

3.4. Comparison with state-of-the-art methods

In this section, the performance of the proposed algorithm is compared with state-of-the-art methods and evaluated in terms of feature matching and SfM-based 3D reconstruction. The former is conducted to quantify the performance of time cost, inlier number, and inlier ratio in feature matching; the latter is utilized to verify the effectiveness in 3D reconstruction.

3.4.1. Feature matching

Feature matching is first evaluated by using four metrics, i.e., *time cost*, *matching speed*, *inlier number*, and *inlier ratio*. The metric *time cost* includes the time consumption in feature matching and outlier removal, and the metric *matching speed* is calculated as the ratio between match pairs

Table 5: The statistical results of matching efficiency for the evaluated methods in terms of time cost and matching speed.

Method	Time cost (min)			Matching speed (pairs/s)		
	Dataset 1	Dataset 2	Dataset 3	Dataset 1	Dataset 2	Dataset 3
ColMap-CPU	258.4	309.8	2064.9	4.0	3.6	3.0
ColMap-GPU	3.4	3.6	71.7	302.4	315.9	85.2
AliceVision	22.7	24.6	155.3	61.3	58.5	55.8
TLBDS	11.3	12.1	70.8	91.1	93.7	86.4
Metashape	8.3	9.2	57.0	33.0	38.9	20.3
Pix4Dmapper	21.0	10.9	136.7	41.0	54.6	30.2
Ours	3.0	3.1	26.7	340.8	362.1	229.0

and time costs; the metrics *inlier number* and *inlier ratio* represent the average true matches and the average number ratio between inliers and initial matches over all match pairs, respectively. In this test, six algorithms are used for performance evaluation, i.e., ColMap-GPU, ColMap-CPU, AliceVision, TLBDS, Metashape, and Pix4Dmapper. For unbiased comparison, the maximum number of matches is configured as 8,192 in Metashape and Pix4Dmapper as that used in the other algorithms.

Table 5 presents the statistical results of time cost and matching speed of all the evaluated algorithms, and Figure 10 plots matching speed for a visual comparison. Considering the metric time cost, ColMap-CPU has the lowest efficiency, which is 258.4 mins, 309.8 mins, and 2064.9 mins for the three datasets, respectively. The main reason is the usage of multi-core CPU for ANN-based feature matching. When accelerated by CPU-based cascade hashing, the time cost of AliceVision obviously decreases to 22.7 mins, 24.6 mins, and 155.3 mins with a speedup ratio of 11.4, 12.6, and 13.3 for the three datasets, respectively. Furthermore, by using the GPU-based cascade hashing, the efficiency of TLBDS is then accelerated by approximately two times when compared with that of AliceVision. Therefore, the test results verify the effectiveness of cascade hashing for feature matching.

For the further analysis, we can see that: (1) the time cost of ColMap-GPU is approximately one third of that in TLBDS for datasets 1 and 2, while they have almost the same time cost in dataset 3. The main reason is due to their different data schedule strategies. In TLBDS, images are ordered according to their connections and are sequentially fed into GPU

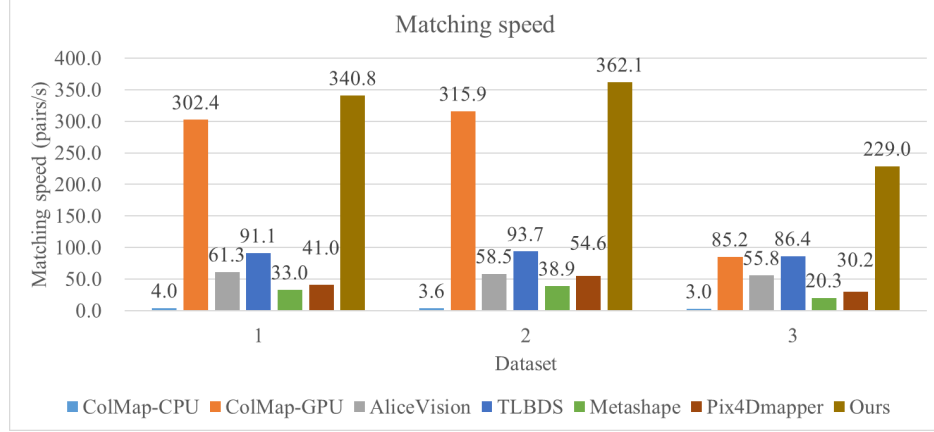


Figure 10: The feature matching speed of all evaluated methods.

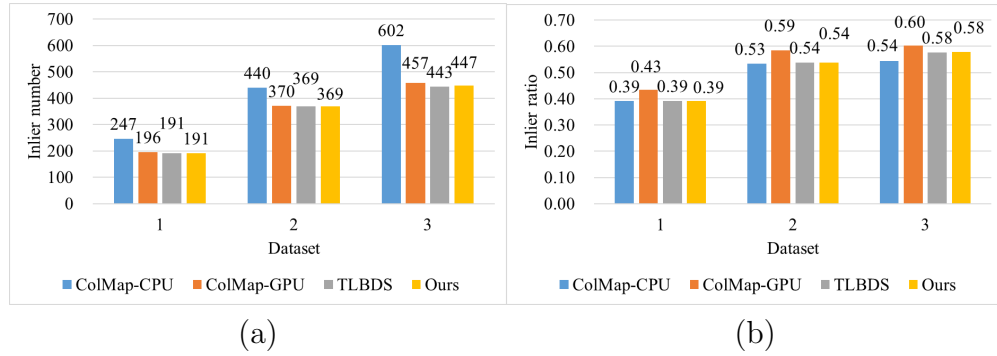


Figure 11: The comparison of inlier number and inlier ratio for the evaluated algorithms: (a) inlier number; (b) inlier ratio.

during feature matching. It causes a lower usage ratio of GPU. On the contrary, ColMap-GPU divides match pairs into blocks that are fed into GPU at one time, which increases overall usage ratio of GPU. However, as the data schedule strategy in ColMap-GPU does not consider image connections, redundant data IO becomes serious for the large-scale dataset 3; (2) compared with TLBDS and ColMap-GPU, the proposed algorithm achieves the highest efficiency for the three datasets, whose time cost is 3.0 mins, 3.1 mins, and 26.7 mins, respectively. The main reason can be explained by the MBR-based data schedule strategy, which considers the usage ratio of GPU to increase efficiency and image connections to decrease IO burden.

Figure 11 presents the comparison in terms of inlier number and in-

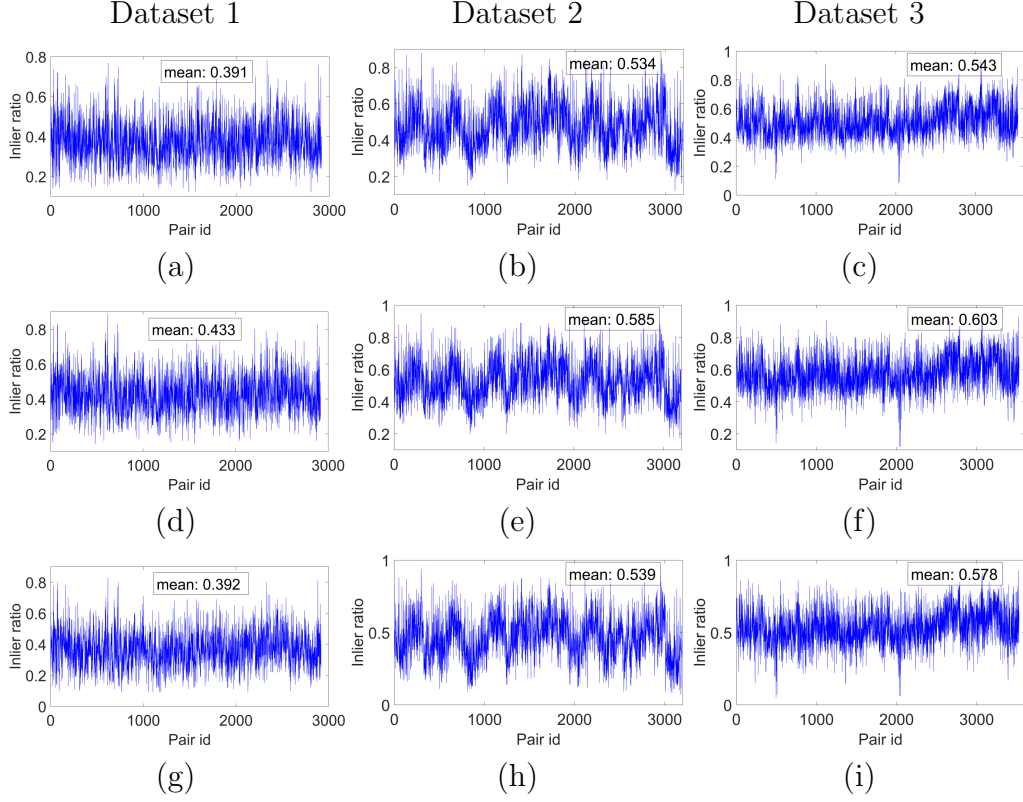


Figure 12: The individual inlier ratio for the three datasets: (a), (b) and (c) for ColMap-CPU; (d), (e) and (f) for ColMap-GPU; (g), (h) and (i) for the proposed algorithm.

lier ratio. Noticeably, these two metrics are not calculated for AliceVision, Metashape, and Pix4Dmapper since only the executable application is utilized in this test. It is shown that for the metric *inlier number*, ColMap-GPU, TLBDS, and the proposed algorithm achieve comparable performance, which is relatively lower than that of ColMap-CPU. For the metric *inlier ratio*, ColMap-GPU achieves the highest performance, which is 0.43, 0.59, and 0.60 for the three datasets. In addition, Figure 12 presents the individual plot of the inlier ratio for the three datasets. Since TLBDS uses the same cascade hashing for feature matching, only the result of the proposed algorithm is analyzed. We can see that the proposed algorithm achieves better performance compared with ColMap-CPU, and evaluated methods have almost consistent change in inlier ratios for all match pairs. In conclusion, the proposed algorithm achieves speedup ratios ranging from 77.0 to 100.0 for feature matching

Table 6: The statistical results of relative BA without GCPs in terms of time cost, the number of registered images, and the number of reconstructed 3D points.

Metric	Method	Dataset 1	Dataset2	Dataset 3
Time cost (min)	ColMap-GPU	13.9	46.1	703.2
	TLBDS	14.8	44.6	714.3
	Metashape	41.8	69.9	—
	Pix4Dmapper	234.2	352.4	—
	Ours	13.9	52.4	669.5
#Registered images	ColMap-GPU	3,736	4,029	21,624
	TLBDS	3,734	4,027	21,349
	Metashape	3,743	4,029	—
	Pix4Dmapper	3736	4027	—
	Ours	3,728	4,027	21,627
#3D points memory costs	ColMap-GPU	874,869	1,340,548	7,698,043
	TLBDS	898,650	1,394,779	8,063,822
	Metashape	2,824,443	2,532,249	—
	Pix4Dmapper	4,407,343	5,206,527	—
	Ours	896,669	1,403,623	8,100,207

compared with traditional KD-Tree based matching methods and provides comparable matching results for subsequent SfM reconstruction.

3.4.2. SfM-based 3D reconstruction

SfM-based 3D reconstruction is then executed by using the obtained feature matches. In general, the performance of SfM-based 3D reconstruction is affected by the inlier number and correspondence distribution over image planes, which can be utilized to evaluate the quality of feature matching. SfM-based 3D reconstruction can be executed without GCPs for relative orientation and with GCP for absolute orientation. For relative BA without GCPs, SfM is used to compare the efficiency and completeness of reconstructed models, in which the efficiency is quantified by time costs, and the completeness is measured by the number of registered images and 3D points. In this test, the parallel SfM solution proposed in Jiang et al. (2024) is used as the engine for ColMap-GPU, TLBDS, and the proposed algorithm.

Table 6 presents the statistical results of relative BA without GCPs for

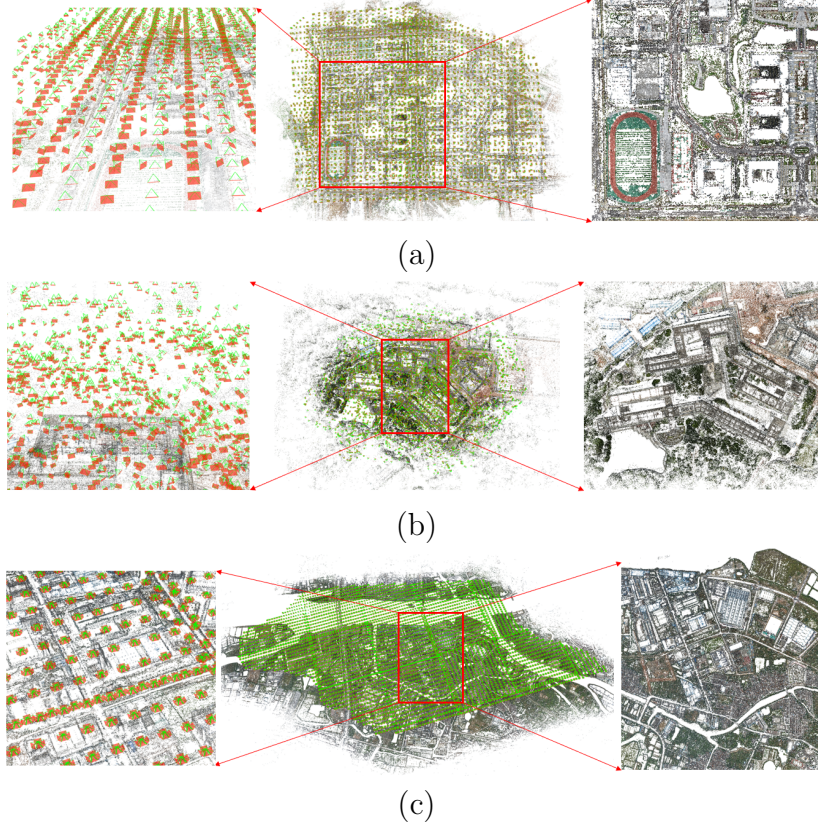


Figure 13: SfM reconstruction results of the three datasets: (a) dataset 1; (b) dataset 2; (c) dataset 3. The sub-figures from the left to right side represents oriented camera poses, entire SfM reconstruction, and detailed 3D points, respectively.

the three datasets. It is shown that except for the two commercial software packages Metashape and Pix4Dmapper, all the other algorithms have comparable time costs consumed in the three datasets, which are 13.9 mins, 52.4 mins, and 669.5 mins for the proposed algorithm. The same findings can also be observed from the metric of the number of registered images, except for TLBDS in dataset 3. For the metric of the number of 3D points, more 3D points are reconstructed in Metashape and Pix4Dmapper since they use different feature detection and matching strategies. For the further comparison between ColMap-GPU and the proposed algorithm, we can see that more 3D points are resumed in the proposed algorithm although almost the same number of images are registered in these two algorithms. The main reason

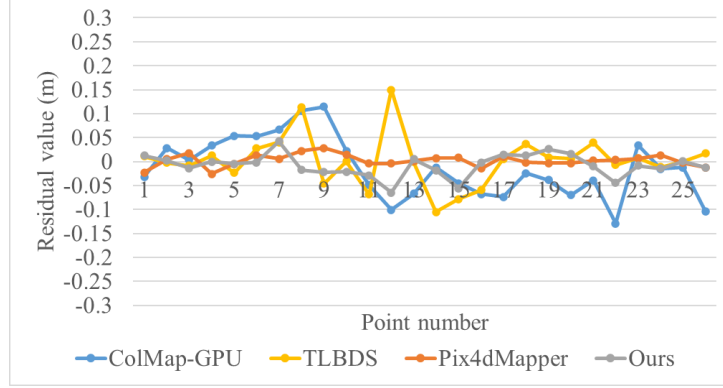
Table 7: The statistical results of absolute BA with GCPs for dataset 2.

Method	Max (m)			Mean (m)			Std.dev. (m)		
	X	Y	Z	X	Y	Z	X	Y	Z
ColMap-GPU	0.129	0.101	0.196	0.054	0.050	0.085	0.063	0.058	0.063
TLBDS	0.150	0.151	0.193	0.034	0.050	0.085	0.053	0.067	0.059
Pix4dMapper	0.028	0.036	0.048	0.010	0.012	0.015	0.013	0.016	0.019
Ours	0.065	0.123	0.096	0.018	0.026	0.037	0.024	0.040	0.037

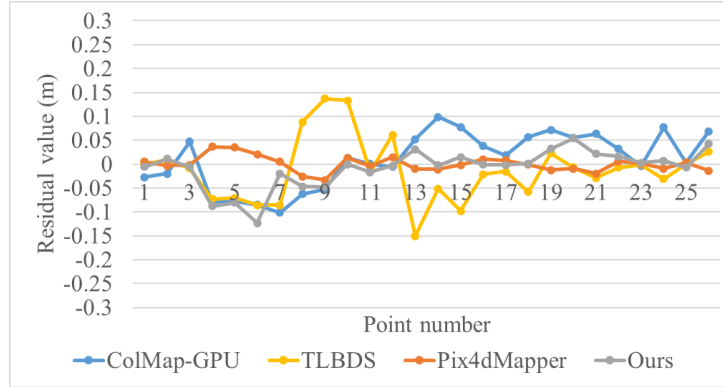
can be explained by the guided feature matching in cascade hashing that improves correspondence distribution. For visual inspection, the reconstructed 3D models are presented in Figure 13. In conclusion, the proposed algorithm can provide reliable and enough feature matches for SfM reconstruction.

With GCPs aided SfM reconstruction, absolute orientation can be conducted to evaluate model geo-referencing accuracy. In this test, three evenly distributed GCPs among the 26 GCPs surveyed in dataset 2 are used as control points for model geo-referencing, and the others are used as check points for accuracy evaluation. The residual is calculated as the positioning offset between estimated model points and corresponding check points. Besides, three metrics, i.e., *Max*, *Mean*, and *Std.dev*, are used for performance evaluation, which indicates the maximum, average, and standard deviation of residuals in the X, Y, and Z directions, respectively.

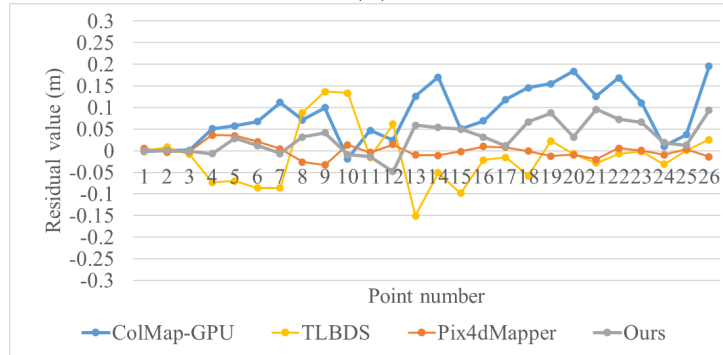
Table 7 presents the statistical results of absolute BA with GCPs, and Figure 14 shows the residual plots. We can conclude that: (1) Pix4dMapper achieves the highest precision among all evaluated algorithms, whose *Std.dev* respectively reaches 0.013 m, 0.016 m, and 0.019 m in the X, Y, and Z directions; (2) TLBDS and ColMap-GPU have comparable precision in the Y and Z directions, while TLBDS achieves higher precision in the X direction; (3) the proposed algorithm ranks second among all evaluated methods, and its precision is 0.024 m, 0.040 m, and 0.037 m in the three directions. It can also be verified by the consistent residual plots shown in Figure 14. Considering that the GSD of dataset 2 is 1.2 cm, the geo-referencing accuracy of the proposed algorithm is better than 2.0 and 3.5 times the GSD value in the horizontal and vertical directions, respectively. Thus, the proposed algorithm can be an efficient and reliable solution for feature matching of large-scale UAV images.



(a)



(b)



(c)

Figure 14: The residual plots after absolute BA by using GCPs in dataset 2: (a) the residual plot in the X axis; (b) the residual plot in the Y axis; (c) the residual plot in the Z axis.

4. Conclusions

This study proposes a matrix band reduction-based GPU data schedule for fast feature matching of UAV images. The core idea is to divide the whole dataset into blocks based on the matrix band reduction and achieve efficient feature matching via GPU-accelerated cascade hashing. First, by using the VLAD-HNSW image retrieval technique, a view graph is created to establish image connections, which is then divided into compact blocks via the matrix band reduction based data schedule strategy. The data schedule strategy adapts well to the connection structure of images and the volume of GPU memory. Second, guided by the generated blocks, feature matching is executed sequentially based on GPU-accelerated cascade hashing, in which initial candidate matches are refined by combining SAO-based local constraint and RANSAC-based global verification in outlier removal. Finally, the proposed algorithm is evaluated and compared by using large-scale UAV datasets. The experimental results demonstrate that the proposed solution can achieve efficient feature matching with tens to hundreds speedup ratios and provide reliable matches for SfM-based 3D reconstruction.

Acknowledgments

This research was funded by the National Natural Science Foundation of China (Grant No. 42371442), and the Hubei Provincial Natural Science Foundation of China (Grant No. 2023AFB568).

References

- Agisoft, 2024. Agisoft metashape homepage. <http://www.agisoft.com>. Accessed: 2024-9-3.
- Cheng, J., Leng, C., Wu, J., Cui, H., Lu, H., 2014. Fast and accurate image matching with cascade hashing for 3d reconstruction, in: Proceedings of the IEEE conference on computer vision and pattern recognition, pp. 1–8.
- Gibbs, N.E., Poole, Jr, W.G., Stockmeyer, P.K., 1976. An algorithm for reducing the bandwidth and profile of a sparse matrix. SIAM Journal on Numerical Analysis 13, 236–250.

- Griwodz, C., Calvet, L., Halvorsen, P., 2018. Popsift: A faithful sift implementation for real-time applications, in: Proceedings of the 9th ACM Multimedia Systems Conference, pp. 415–420.
- Griwodz, C., Gasparini, S., Calvet, L., Gurdjos, P., Castan, F., Maujean, B., De Lillo, G., Lanthony, Y., 2021. Alicevision meshroom: An open-source 3d reconstruction pipeline, in: Proceedings of the 12th ACM multimedia systems conference, pp. 241–247.
- Hartmann, W., Havlena, M., Schindler, K., 2016. Recent developments in large-scale tie-point matching. *ISPRS Journal of Photogrammetry and Remote Sensing* 115, 47–62.
- Havlena, M., Schindler, K., 2014. Vocmatch: Efficient multiview correspondence for structure from motion, in: European Conference on Computer Vision, Springer. pp. 46–60.
- Hou, Q., Xia, R., Zhang, J., Feng, Y., Zhan, Z., Wang, X., 2023. Learning visual overlapping image pairs for sfm via cnn fine-tuning with photogrammetric geometry information. *International Journal of Applied Earth Observation and Geoinformation* 116, 103162.
- Ji, S., Zeng, C., Zhang, Y., Duan, Y., 2023. An evaluation of conventional and deep learning-based image-matching methods on diverse datasets. *The Photogrammetric Record* 38, 137–159.
- Jiang, S., Jiang, C., Jiang, W., 2020a. Efficient structure from motion for large-scale uav images: A review and a comparison of sfm tools. *ISPRS Journal of Photogrammetry and Remote Sensing* 167, 230–251.
- Jiang, S., Jiang, W., 2020. Efficient match pair selection for oblique uav images based on adaptive vocabulary tree. *ISPRS Journal of Photogrammetry and Remote Sensing* 161, 61–75.
- Jiang, S., Jiang, W., Guo, B., 2022a. Leveraging vocabulary tree for simultaneous match pair selection and guided feature matching of uav images. *ISPRS Journal of Photogrammetry and Remote Sensing* 187, 273–293.
- Jiang, S., Jiang, W., Guo, B., Li, L., Wang, L., 2021a. Learned local features for structure from motion of uav images: A comparative evaluation. *IEEE*

- Journal of Selected Topics in Applied Earth Observations and Remote Sensing 14, 10583–10597.
- Jiang, S., Jiang, W., Huang, W., Yang, L., 2017. Uav-based oblique photogrammetry for outdoor data acquisition and offsite visual inspection of transmission line. Remote Sensing 9, 278.
- Jiang, S., Jiang, W., Li, L., Wang, L., Huang, W., 2020b. Reliable and efficient uav image matching via geometric constraints structured by delaunay triangulation. Remote Sensing 12, 3390.
- Jiang, S., Jiang, W., Wang, L., 2021b. Unmanned aerial vehicle-based photogrammetric 3d mapping: A survey of techniques, applications, and challenges. IEEE Geoscience and Remote Sensing Magazine 10, 135–171.
- Jiang, S., Li, Q., Jiang, W., Chen, W., 2022b. Parallel structure from motion for uav images via weighted connected dominating set. IEEE Transactions on Geoscience and Remote Sensing 60, 1–13.
- Jiang, S., Ma, Y., Liu, J., Li, Q., Jiang, W., Guo, B., Li, L., Wang, L., 2023. Efficient match pair retrieval for large-scale uav images via graph indexed global descriptor. IEEE Journal of Selected Topics in Applied Earth Observations and Remote Sensing 16, 9874–9887.
- Jiang, S., You, K., Chen, W., Weng, D., Li, Y., 2024. 3d reconstruction of spherical images based on incremental structure from motion. International Journal of Remote Sensing 45, 2596–2621.
- Johnson, J., Douze, M., Jégou, H., 2019. Billion-scale similarity search with gpus. IEEE Transactions on Big Data 7, 535–547.
- Li, Q., Huang, H., Yu, W., Jiang, S., 2023. Optimized views photogrammetry: Precision analysis and a large-scale case study in qingdao. IEEE Journal of Selected Topics in Applied Earth Observations and Remote Sensing 16, 1144–1159.
- Lloyd, S., 1982. Least squares quantization in pcm. IEEE transactions on information theory 28, 129–137.
- Lowe, D.G., 2004. Distinctive image features from scale-invariant keypoints. International journal of computer vision 60, 91–110.

- Lu, L., Zhang, Y., Tao, P., 2016. Geometrical consistency voting strategy for outlier detection in image matching. *Photogrammetric Engineering and Remote Sensing* 82, 559–570.
- Nister, D., Stewenius, H., 2006. Scalable recognition with a vocabulary tree, in: 2006 IEEE Computer Society Conference on Computer Vision and Pattern Recognition (CVPR’06), Ieee. pp. 2161–2168.
- Pix4Dmapper, 2024. Pix4dmapper homepage. <https://www.pix4d.com>. Accessed: 2024-9-3.
- Remondino, F., Gerke, M., 2015. Oblique aerial imagery—a review, in: *Photogrammetric week*, pp. 75–81.
- Rublee, E., Rabaud, V., Konolige, K., Bradski, G., 2011. Orb: An efficient alternative to sift or surf, in: 2011 International conference on computer vision, Ieee. pp. 2564–2571.
- Schonberger, J.L., Frahm, J.M., 2016. Structure-from-motion revisited, in: *Proceedings of the IEEE conference on computer vision and pattern recognition*, pp. 4104–4113.
- Schönberger, J.L., Fraundorfer, F., Frahm, J.M., 2014. Structure-from-motion for mav image sequence analysis with photogrammetric applications. *The International Archives of the Photogrammetry, Remote Sensing and Spatial Information Sciences* 40, 305–312.
- Vedaldi, A., Fulkerson, B., 2010. Vlfeat: An open and portable library of computer vision algorithms, in: *Proceedings of the 18th ACM international conference on Multimedia*, pp. 1469–1472.
- Wang, X., Xiang, H., Niu, W., Mao, Z., Huang, X., Zhang, F., 2023. Oblique photogrammetry supporting procedural tree modeling in urban areas. *ISPRS Journal of Photogrammetry and Remote Sensing* 200, 120–137.
- Wu, C., 2011. Siftgpu: A gpu implementation of scale invariant feature transform (sift)(2007). URL <http://cs.unc.edu/~ccwu/siftgpu>.
- Xu, T., Sun, K., Tao, W., 2017. Gpu accelerated image matching with cascade hashing, in: *Computer Vision: Second CCF Chinese Conference, CCCV 2017, Tianjin, China, October 11–14, 2017, Proceedings, Part I*, Springer. pp. 91–101.

- Yao, H., Qin, R., Chen, X., 2019. Unmanned aerial vehicle for remote sensing applications—a review. *Remote Sensing* 11, 1443.
- Zhang, Q., Zheng, S., Zhang, C., Wang, X., Li, R., 2023. Efficient large-scale oblique image matching based on cascade hashing and match data scheduling. *Pattern Recognition* 138, 109442.
- Zheng, J., Fu, H., Li, W., Wu, W., Yu, L., Yuan, S., Tao, W.Y.W., Pang, T.K., Kanniah, K.D., 2021. Growing status observation for oil palm trees using unmanned aerial vehicle (uav) images. *ISPRS Journal of Photogrammetry and Remote Sensing* 173, 95–121.